SIGNAL-PROCESSING ALGORITHM DEVELOPMENT FOR THE ACLAIM SENSOR

Final Report: Gust Detection

prepared for

NASA Dryden Flight Research Center
ACLAIM program

under
Cooperative Agreement No. NCC4-0014

Alabama A&M University
Office of Research and Development
Normal, Alabama
35762-0411

Table of Contents

SIGNAL-PROCESSING ALGORITHM DEVELOPMENT FOR THE ACLAIM SENSOR

Final Report: Gust Detection

Scott von Laven

Introduction

As described in previous ACLAIM reports[1-2], the ACLAIM program is a demonstration of the feasibility of using an on-board look-ahead lidar to measure wind velocities. Indications are that such a lidar has sufficient range to prevent engine unstart in aircraft such as the High-Speed Civil Transport (HSCT). A change in Mach number of approximately five per cent is considered sufficient to cause unstart if it occurs on a time scale of seconds or less, as shown in Fig. 1[3].

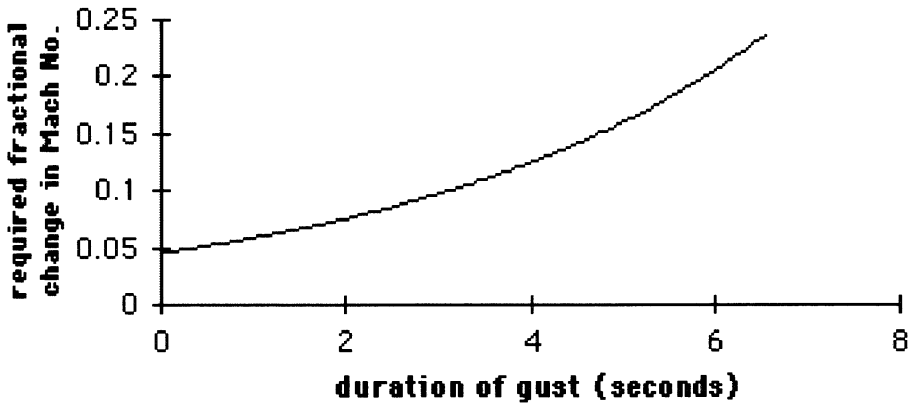

Fig. 1. Gust magnitude required to cause unstart.

Our general approach to improving the detection of wind-field disturbances, such as a sudden change in Mach number, is, first, to attempt to determine characteristic patterns is the wind field and, second, to use that information to evaluate the probability that partial events might grow into full events (Fig. 2). Throughout this report wind-field disturbances may also be referred to as "events", or in some circumstances "gusts".

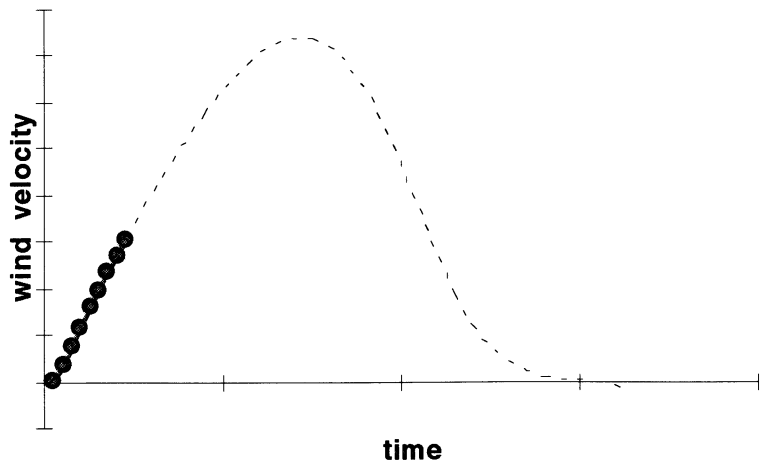

Fig. 2. An example of a signal (circles), referred to as a partial event or precursor) that might indicate a significant wind-field event or gust (dashes).

In consultation with other ACLAIM participants, a detailed approach involving empirical orthonormal functions (EOFs) was pursued and is summarized in the next section. In the subsequent section we describe wind-field simulations that show how an event-detection scheme employing partial events (precursors) might be calibrated.

Empirical Orthonormal Functions

EOF's are eigenfunctions (ϕ_n) obtained from an arbitrary data set by solving the eigenvalue equation associated with data set's two-point correlation function (K). Explicitly we solve

$$\int K(x,y)\phi_n(x)dx = \lambda_n \phi_n(y), \qquad (1)$$

for the first few ϕ_n, where the λ_n are the eigenvalues and

$$K(x,y) = \langle f(x) f(y) \rangle, \qquad (2)$$

and x and y both refer to time (or, equivalently, the axial coordinate). References 4 and 5 discuss EOFs in a context similar to ACLAIM.

The example presented in Figures 3 and 4 illustrates the concept of EOFs.

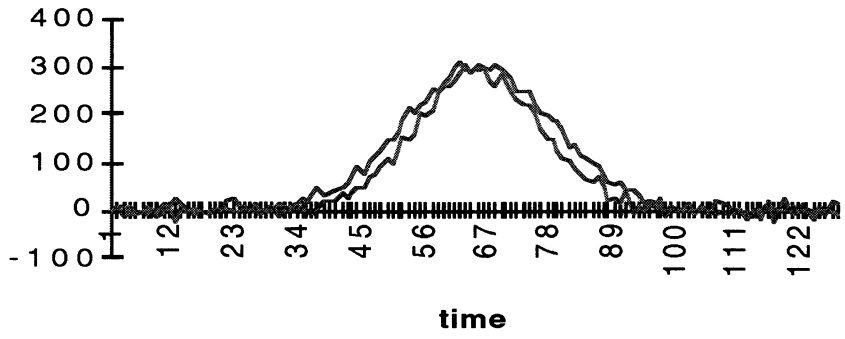

Fig. 3. A data series was generated by allowing the width parameter of the Gaussian component of the signal to drift from the lower value (green) to the upper value (red) and adding a small noise component.

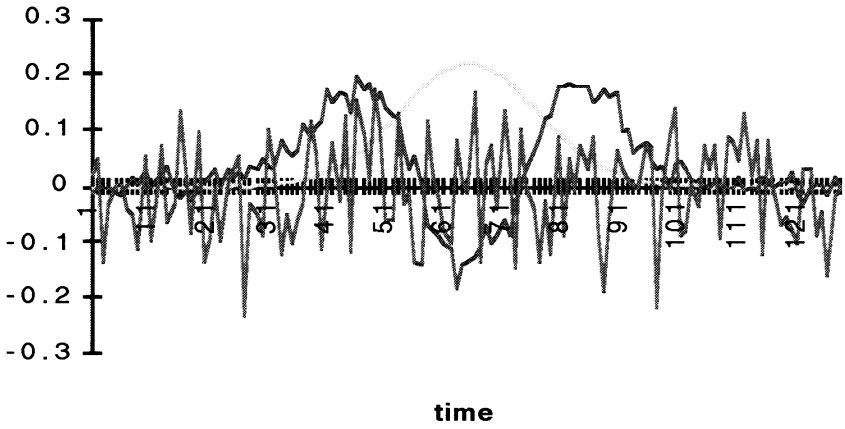

Fig. 4. First 3 eigenfunctions extracted from the data shown in Fig. 3. The large amplitude (i.e., eigenvalue) of the second eigenfunction (red) is a result of the drift in the width of the Gaussian.

For convenience, we also include a flow diagram from a previous report[2] (Fig. 5). The diagram indicates the role of the EOFs (also referred to as coherent structures in the earlier report) in ACLAIM signal processing from a software-engineering point of view.

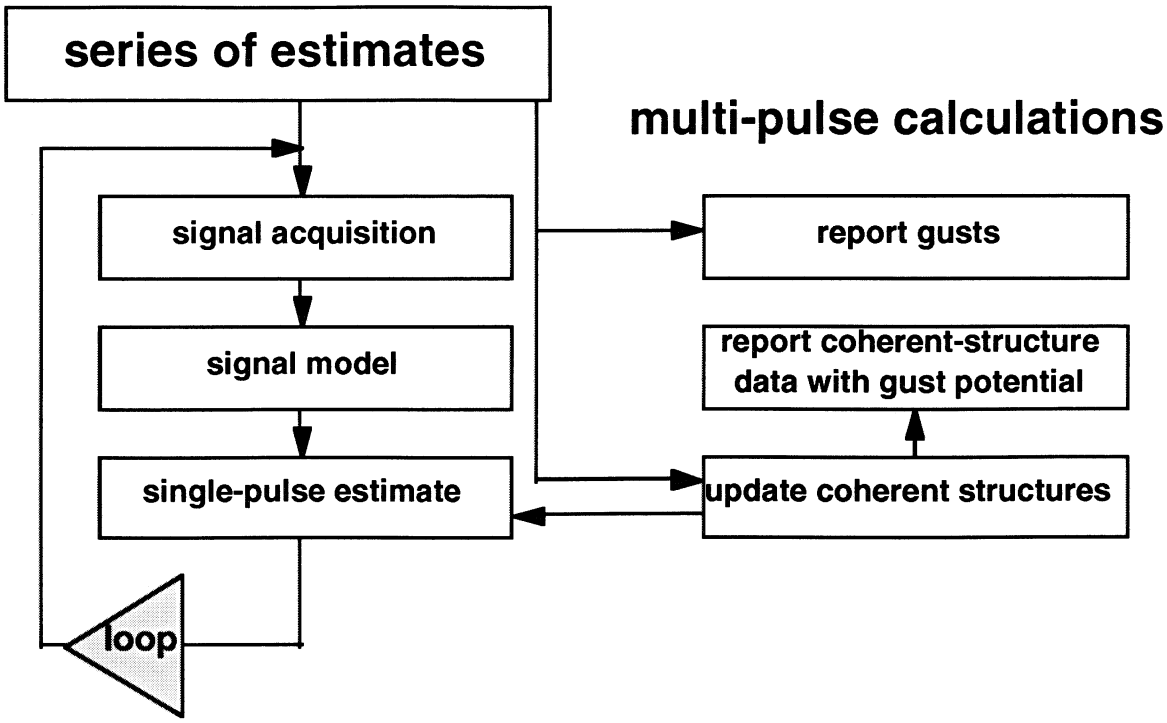

Fig. 5. Flow of EOF information.

Gust Detection Schemes

This section focuses on the block in Fig. 5 labeled "report data with gust potential". By having gust potential we mean that the data is somehow associated with a characteristic pattern in the wind field and that we can establish a probability that a gust meeting particular criteria will occur within a given time. It will be assumed that characteristic patterns are available either through the EOF procedure described above or by other means. We describe first a procedure for reporting the gust potential of data sets. These potentials are then correlated with the subsequent observation of gusts.

Characterization of data sets

Our simulated wind fields consist of sets of pulses with parameters like those seen at the output of the front-end receiver, complete with Gaussian noise. Pulses consist usually of 32, 64, or (for algorithm test purposes) 128 samples as in the example of Fig. 6.

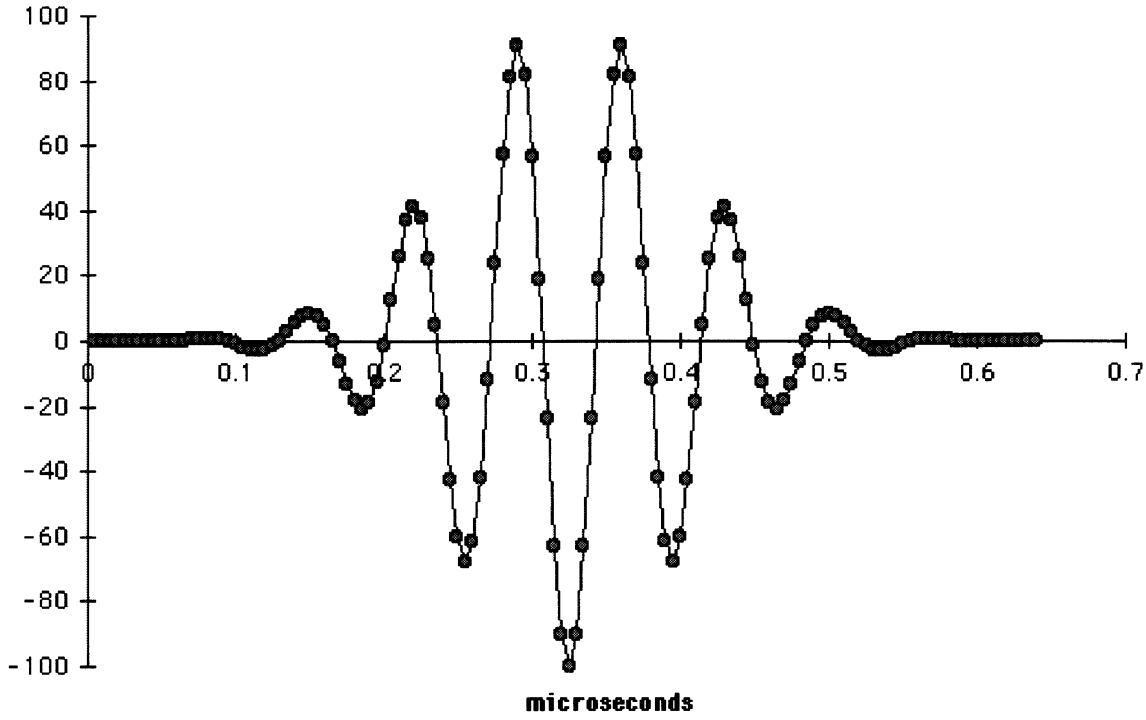

Fig. 6 Simulated pulse (without noise) with a frequency (after mixing) of 14.1 MHz.

Sampling rates range from 50 to 500 Mhz, and pulse durations range from 100 to 300 nanoseconds. Sets typically consist of 25 pulses each. Frequency estimation is applied to individual pulses, and sets are examined for frequency variations that meet specified criteria. For example, if we wish to report gusts of a certain magnitude, we set the appropriate threshold for frequency variation within a set and perhaps a maximum pulse count within which that variation must occur. If a frequency variation with appropriate parameters is observed, a gust is reported. Multiple sets can be used to generate statistics. Pulse sets can be repeated with essentially the same parameters except for the seed of the random number generator responsible for the noise. The ratio of pulse sets containing a gust to the total number of pulse sets then becomes a gust probability. If we then want to determine the sensitivity of gust detection probability to parameters such as gust amplitude, even larger groupings of pulses are necessary.

Gust probability

To demonstrate the concept of gust probability, the signal generator is programmed to look up the signal frequency for successive pulses from a file, which can be prepared as desired to produce gusts of any desired profile. Figures 7a and 7b display the estimator output for two series of pulse sets, each with different random noise between sets, but with the overall noise level higher in Fig. 7b.

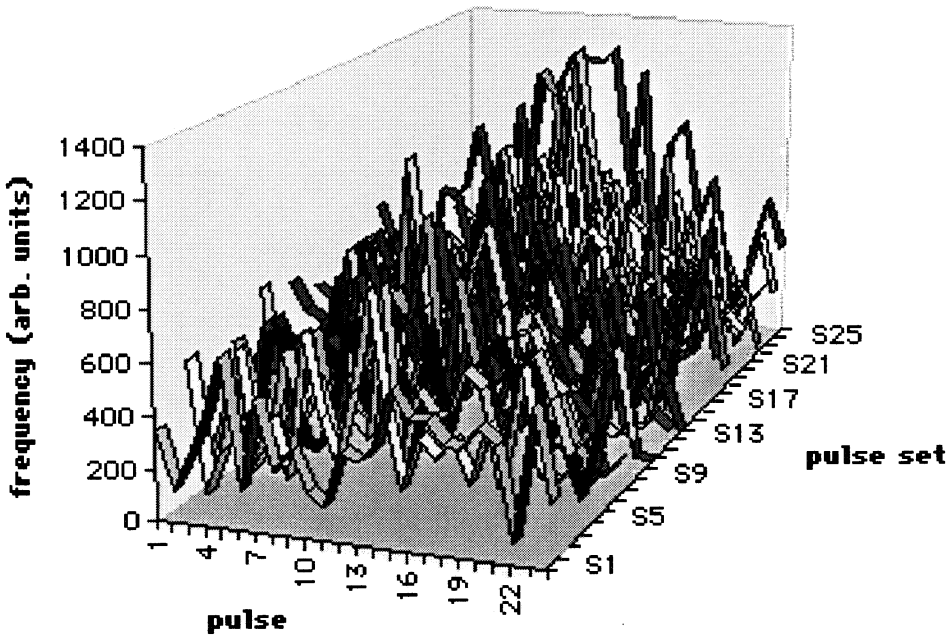

Fig, 7a. Pulse sets with a random, but low, noise level.

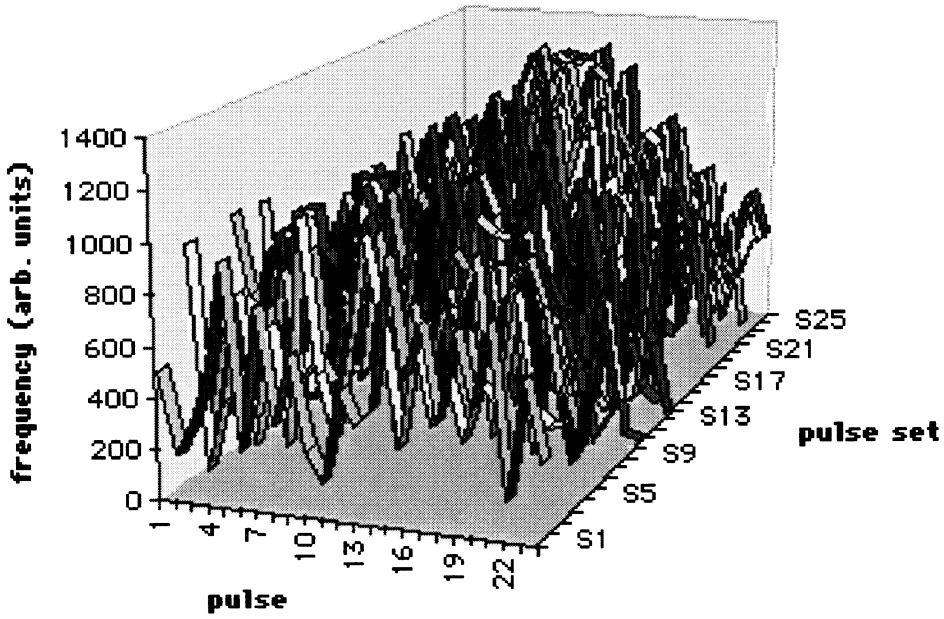

Fig, 7b. Pulse sets with a random high noise level.

Each pulse set is tested for the presence of a gust satisfying the criteria specified for each series of tests. To establish a probability of gust detection a series of pulse sets is generated. The sequence of pulses within a pulse set is shifted by one pulse each time a

new set is begun such that each series consists of 25 identical pulse sets, except for the permuted order and the noise component. For each set the detection of a gust is assigned a value of 1.0 and non-detection a value of 0.0. These 25 values are averaged over the 25 pulse sets within the series to give a probability of gust detection.

As we examine the sensitivity of gust-detection probability to various gust characteristics or other external parameters, an entire series of the type described above must be generated for each set of characteristics. In Fig. 8 the upper surface represents gust-detection probability, in this case as a function of both gust amplitude and overall noise level. Each value was obtained through the generation of a series of pulse sets, with the gust and noise amplitudes held constant within each series. A gust was defined as a change in estimated signal of at least 750 (code units) occurring over a pulse separation of more than 2 pulses and less than 20 pulses.

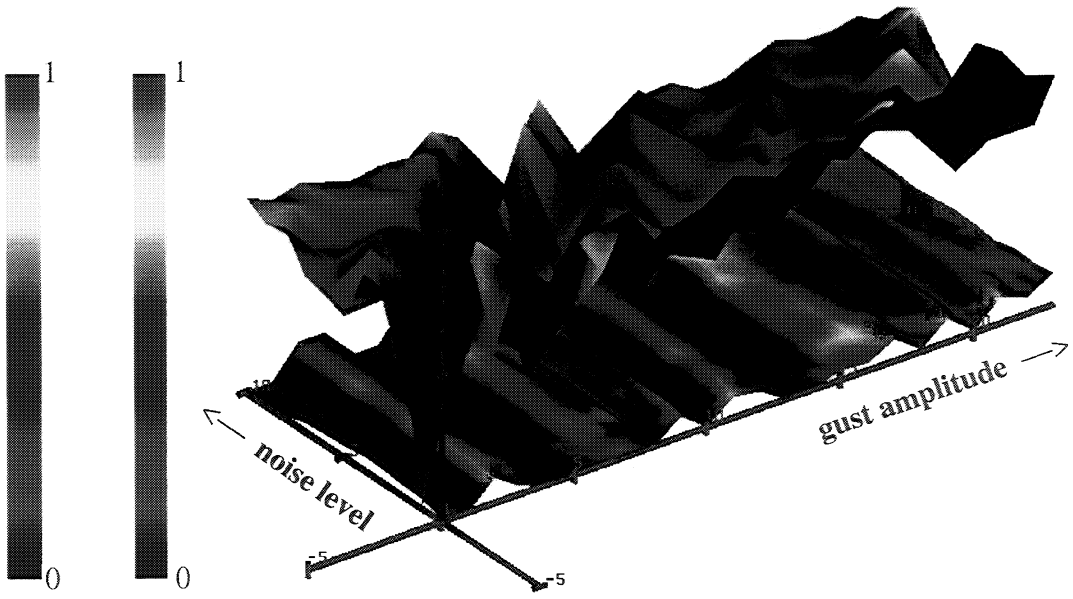

Fig. 8. Gust-detection probability (upper surface and right-hand color legend) and precursor quality (lower surface and left-hand color legend), both functions of gust amplitude and overall noise level.

Precursors

As Fig. 2 suggests, the detection of precursors can increase the time available to respond to gusts. Figure 8 illustrates this concept by allowing us to correlate by eye a measure of the presence of a precursor with gust-detection probability. The measure we have used, and referred to as precursor quality, is an overlap integral q

$$q = \frac{\int f(t)g(t)dt}{\int f(t)f(t)dt} \qquad (3)$$

where g(t) represents the leading edge of the "known" gust profile and f(t) is the estimated signal. In the results presented here g(t) is simply the profile of the input to the signal generator. In practice g(t) would be an EOF or closely related function. Before the integral q is evaluated, f(t) and g(t) must be temporally aligned. This is currently accomplished by means of a least-squares fit.

In examining Fig. 8 we see that, for low noise, gust-detection probability seems to increase slightly (and unevenly) with respect to gust amplitude and seems to be very roughly correlated with the precursor quality. For high noise, as we might expect, no such general descriptions, however rough, seem to apply. Incorporating percursor quality into our detection scheme is simply a matter of applying an additional test to the frequency estimates. Presumably, after a period of calibration, the other tests could be dropped, and we would be with a detection scheme capable of operating with fewer pulses.

Sensitivity to Gust Parameters

Setting precursors aside for now, we examine the performance of our "raw" gust detection scheme. The data presented in Fig. 9 is the result of testing to determine whether stronger gusts are more easily detected than weaker gusts. At the same time different levels of receiver noise are introduced. The noise-level scale is linear, with relative values ranging from one to ten for all of the data in this section. The signal in all cases has a relative amplitude (at the receiver) of three, such that the signal-to-noise ratio ranges from 3:1 to 3:10.

Initially, (no-averaging case) no sensitivity to gust amplitude is exhibited over this parameter range. (We believe the rapid oscillations with respect to gust amplitude to be an artifact of our method of pulse-set preparation, and that these oscillations could be eliminated with further refinement.) If we apply gust detection to temporally averaged frequency estimates of the same input signal, sensitivity to gust amplitude begins to emerge. The averaging has the effect of reducing sensitivity overall, such that only the stronger gusts are detected for this set of parameters. Adjusting the pass band of the analog front end of the receiver so as to maintain the maximum possible dynamic range at all times would be alternative method of adjusting the sensitivity. With regard to noise level, very little sensitivity is exhibited over the range of values used in this study.

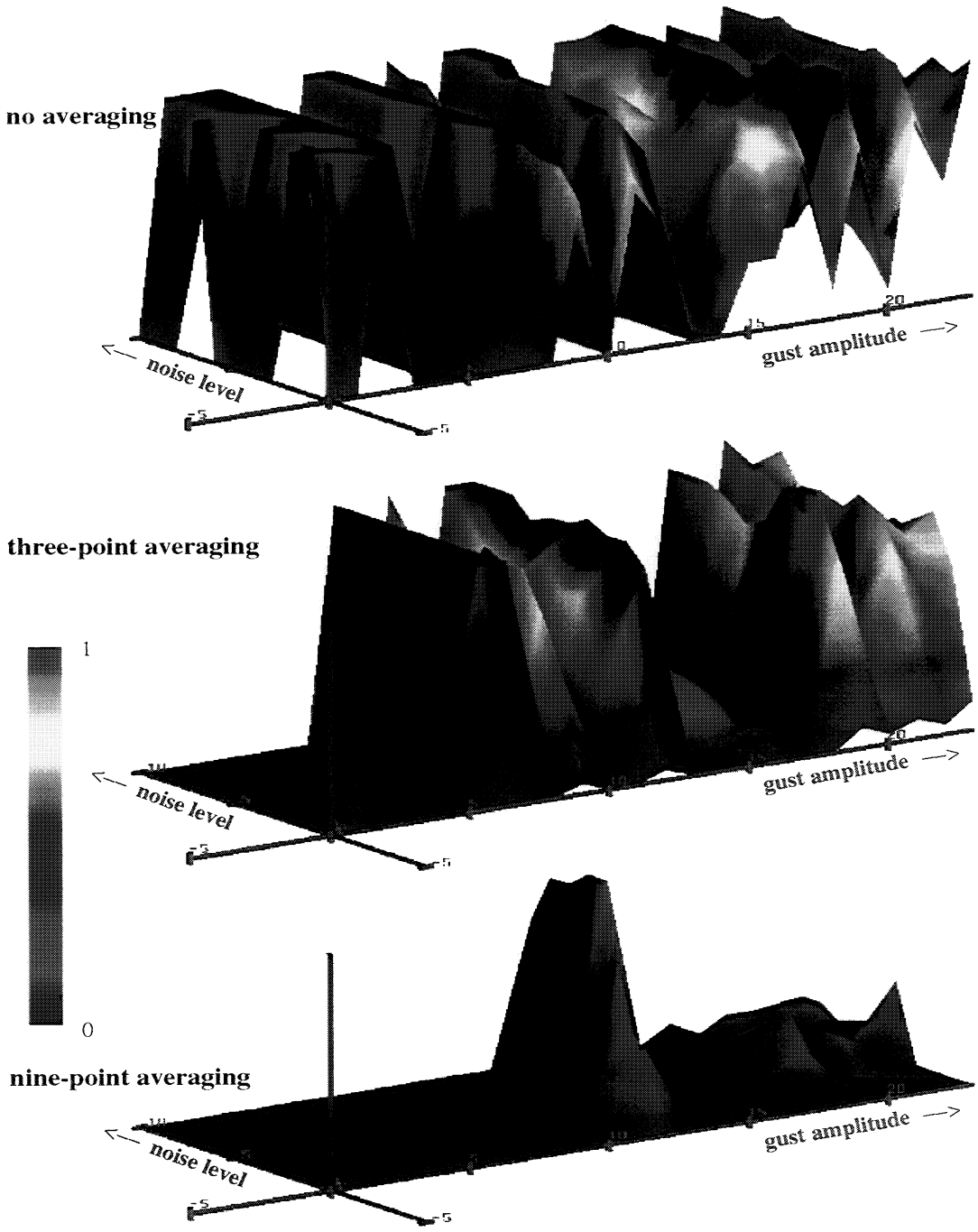

Fig. 9. Gust-detection probability vs. gust amplitude and noise level. The gust amplitude scale represents a series of pulse sets. In this case, pulse set 1 has a relative gust amplitude of 11; pulse set 2 has a relative gust amplitude of 12, and so on up to pulse set 25 with a relative gust amplitude of 35. The different levels of averaging are applied to the frequency estimate before any further processing occurs.

Figure 10 looks at detection sensitivity as a function of gust duration (temporal width). Again, little sensitivity is apparent until averaging is applied. Then we see that shorter

gusts are more easily detected. With respect to noise level, we see, if anything, a higher probability of detection for higher noise levels, possibly corresponding to false alarms.

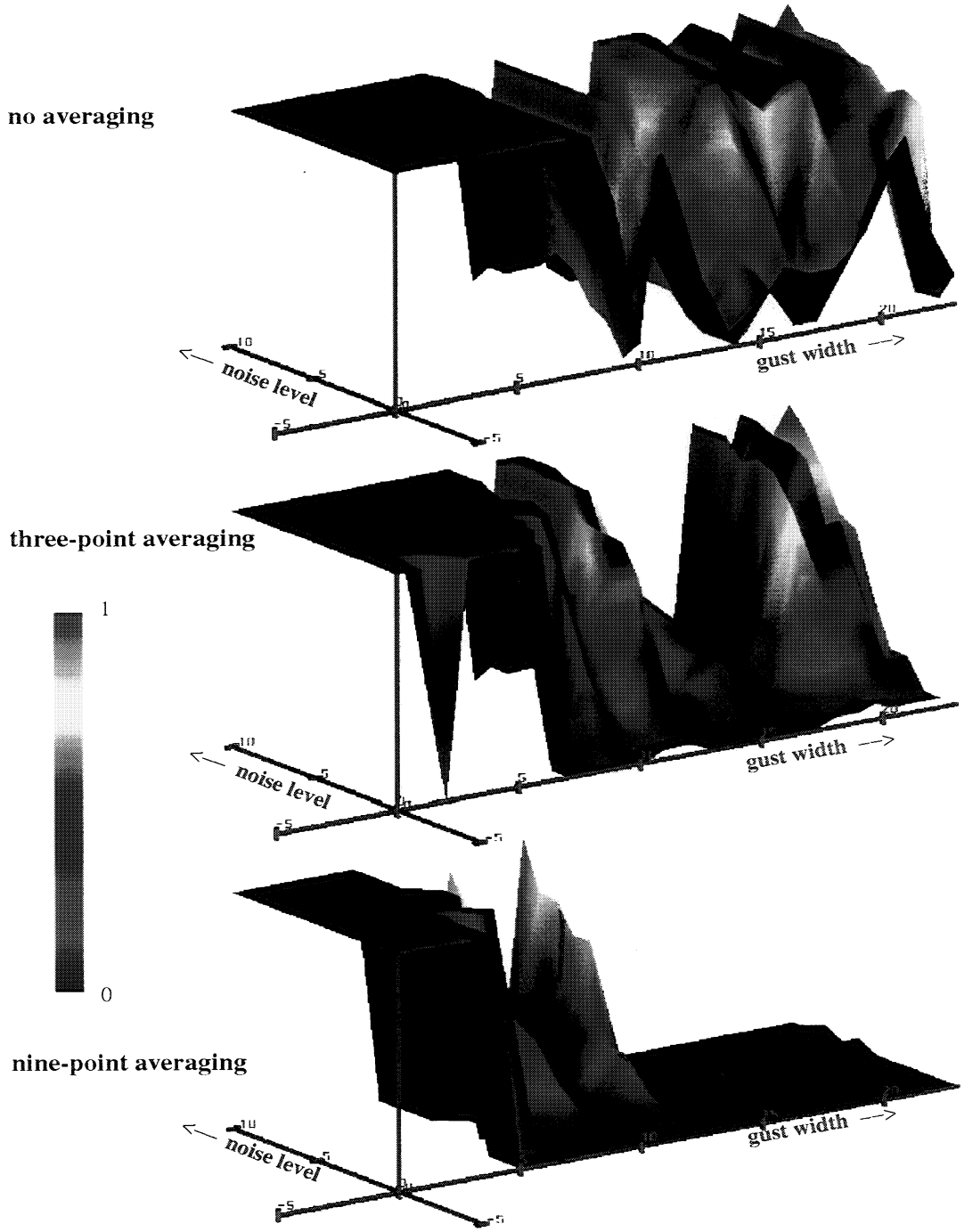

Fig. 10. Gust-detection probability vs. gust width and noise level. The gust-width scale represents a series of pulse sets in manner similar to the gust-amplitude scale of Fig. 9. In this case the range is relatively narrow, with pulse set 1 corresponding to a gust width of roughly three pulses and pulse set 25 corresponding to a gust width of roughly five pulses.

Conclusions

Methods for further minimizing the risk of unstart by making use of previous lidar observations were investigated. EOFs are likely to play an important role in these methods, and a procedure for extracting EOFs from data has been implemented. The new processing methods involving EOFs could range from extrapolation, as discussed above, to more complicated statistical procedures for maintaining low unstart risk.

We have also applied our basic gust-detection scheme to simulated wind-field data and obtained reasonable performance. The extension of this scheme to include precursors (EOF-based or otherwise) is straightforward. Exactly the same procedures are followed up to the point of evaluating a set of frequency estimates against the gust criteria. At this point, precursor quality is simply added as an additional criterion.

Acknowledgments

Useful comments and assistance were obtained from, Alex Thomson, Dave Soreide, Steve Hannon, Dave Bowdle, Rod Frehlich, Steve Johnson, Philip Kromis, Rod Bogue, Grettel von Laven, and Z.T. Deng.

References

1. R. Bogue, H. Bagley, D. Soreide, and D. Bowdle, "Coherent lidar solution for the HSCT supersonic engine inlet unstart problem," *SPIE Proceedings*, **2464**-13, 1995.
2. S. von Laven, "1995 ACLAIM Technical Report", Alabama A&M University, 1995.
3. C. Carlin, Boeing Aerospace Corporation, private communication, 1995.
4. P. Moin and R.D. Moser, "Characteristic-eddy decomposition of turbulence in a channel," *Journal of Fluid Mechanics*, 200, pp. 471-509, 1989.
5. N. Aubry, P. Holmes, J.L. Lumley, and E. Stone, "The dynamics of coherent structures in the wall region of a turbulent boundary layer," *Journal of Fluid Mechanics*, 192, pp. 115-173, 1988.
6. M. Loève, *Probability Theory*, D. Van Nostrand, Princeton, NJ, 1963.
7. J.L. Lumley, "The structure of inhomogeneous turbulent flows," *Atmospheric Turbulence and Radio Wave Propagation*, A.M. Yaglom and V.I. Tatarskii, Eds. Nauka, Moscow, pp. 166-176, 1967.
8. H.A. Panofsky, and J.A. Dutton, *Atmospheric Turbulence, Models and Methods for Engineering Applications*, Wiley, New York, 1984.